Collisional excitation of HNC by He found to be stronger than for structural isomer HCN in experiments at the low temperatures of interstellar space

Brian M. Hays, Divita Gupta, Théo Guillaume, Omar Abdelkader Khedaoui, Ilsa R. Cooke, Franck Thibault, François Lique, Ian R Sims

***Title*:**

Collisional excitation of HNC by He found to be stronger than for structural isomer HCN in experiments at the low temperatures of interstellar space

***Author list*:**

Brian M. Hays,[1] Divita Gupta,[1] Theo Guillaume,[1] Omar Abdelkader Khedaoui,[1] Ilsa R. Cooke,[1] Franck Thibault,[1] François Lique[1] and Ian R. Sims[1,*]

***Affiliations*:**

[1] Univ Rennes, CNRS, IPR (Institut de Physique de Rennes) - UMR 6251, F-35000 Rennes, France.

* e-mail: ian.sims@univ-rennes1.fr

***Abstract*:**

HCN and its unstable isomer HNC are widely observed throughout the interstellar medium, with the HNC/HCN abundance ratio correlating strongly with temperature. In very cold environments HNC can even appear more abundant than HCN. Here, we use a chirped pulse Fourier transform spectrometer to measure the pressure broadening of HCN and HNC, simultaneously formed in situ by laser photolysis and cooled to low temperatures in uniform supersonic flows of helium. Despite the apparent similarity of these systems, we find the HNC–He cross section to be more than twice as big as the HCN–He cross section at 10 K, confirming earlier quantum calculations. Our experimental results are supported by high level scattering calculations and are also expected to apply with para-H_2, demonstrating that HCN and HNC have different collisional excitation properties which strongly influence the derived interstellar abundances.

***Main text*:**

Studying isomeric systems in space offers a tantalizing opportunity to investigate how extreme environments can affect chemically related species. HCN and HNC in the interstellar medium (ISM) are fascinating examples of this. HNC is the higher energy isomer by 62 kJ mol^{-1} with a large ca. 140 kJ mol^{-1} barrier to isomerization.[1–3] HCN is the dominant isomer on Earth, while HNC is only observed in the laboratory as a transient molecule or at very high temperatures.[4–6] In the rarefied environment of space, however, HNC is widely observed.[7] The ubiquity of these molecules and the temperature dependence of the HNC/HCN abundance ratio have been used as a tool to map the temperature of star forming regions[8] and protoplanetary disks.[9] However, enigmatic observations from the 90's have found that despite being less stable than HCN, HNC can appear to be the more abundant isomer in very cold environments, by up to a factor of 5, an intriguing and non-intuitive result.[10]

The kinetics that control the HCN and HNC abundances in the ISM are thought to be dominated by highly exothermic reactions, such as the dissociative recombination of $HCNH^+$ and electrons, that form products with high internal energy, yielding both isomers with near unity ratio.[5,11,12] Destructive chemistry is then thought to preferentially deplete HNC as temperatures rise.[13] This simple model supports the use of the

observed abundance ratio of these molecules as a thermometer,[8] but is not sufficient to explain the enhanced abundance of HNC in certain environments.

The determination of molecular abundances from observational spectra requires knowledge of the population of the rotational energy levels of the interstellar molecules. In the ISM, the density is generally not high enough to maintain local thermodynamic equilibrium conditions. As a consequence, the population of the molecular levels is controlled by the competition between collisional (de-)excitation and radiative processes. Given the similar dipole moments and rotational constants for HCN and HNC, it had been assumed that the excitation conditions (i.e. the populations of the rotational states) were almost identical,[13] and these were computed on the basis of only HCN collisional rate coefficients. The HNC/HCN line intensity ratio then gives, as a first approximation, the HNC/HCN abundance ratio. Because the HNC lines are much stronger than those of HCN in the cold ISM, the HNC/HCN abundance ratio was found to be much greater than 1, in strong disagreement with existing astrochemical models.[10] To explain this, Lique and co-workers proposed that HCN and HNC do not undergo identical collisional excitation, contrary to what had been widely assumed.[14,15] They obtained high level *ab initio* potential energy surfaces (PESs) for HCN and HNC with both He and H_2, the dominant colliders in the cold ISM,[15–18] and performed close-coupling scattering calculations to generate collisional rate coefficients for rotational energy transfer (RET). They observed strong differences between the two isomers and attributed this to a change in anisotropy between the two potentials. When these newly calculated rate coefficients, now differing strongly between these two isomers, are used in conjunction with observational data, significantly lower abundance ratios are found (~1-2), compatible with the predictions of astrochemical models. However, these calculations and their important astrochemical consequences have not yet been supported by any experimental measurements.

While HCN and HNC are readily identified in the ISM, few laboratory experiments are available to confirm the theoretically supported kinetics or RET rates for these molecules. In fact, no experiments of this kind have been performed on HNC, presumably owing to its instability in the laboratory making it impossible to obtain pure samples. While vibrational spectroscopy has been used to examine these isomers in collisional or photodissociative environments,[19,20] only recently has rotational spectroscopy become sensitive enough to allow for the detection of these species through transient experiments.[6,21] Here we describe an experiment to investigate the collisional properties of HCN and HNC with He at low temperatures, combining simultaneous *in situ* generation of HCN and HNC by laser photolysis in continuous uniform supersonic flows of cold He with time-resolved chirped pulse Fourier transform millimeter wave (CPFTmmW) spectroscopy.[22,23] We measure the pressure broadening cross sections for these two systems down to 10 K and thereby verify the theoretically predicted difference in collisional excitation on an absolute scale.

Results

Experimental protocols

The experiments were performed in a recently developed CPUF (Chirped Pulse in Uniform supersonic Flow) apparatus. The CPUF technique was first developed by Suits and coworkers[24] and is based on the cold collisional environment provided by a CRESU (*Cinétique de Réaction en Ecoulement Supersonique Uniforme* or Reaction Kinetics in Uniform Supersonic Flow) apparatus,[25,26] combined with in-situ production of reactive or

transient species by pulsed laser photolysis and CPFTmmW detection. The CPUF apparatus used here differs from the previous version of Suits and co-workers principally in its use of continuous rather than pulsed uniform supersonic flows, giving more precisely defined flow conditions and enabling higher repetition rate pulsed photolysis (100 Hz in this case). It also employs a higher power CPFTmmW spectrometer which is fully described in Hays et al.[27] Fig. 1a shows a schematic diagram representing the essential features of the experiment. Briefly, the cold core of a uniform supersonic flow of He containing trace amounts of vinyl cyanide at temperatures ranging from 10-70 K is illuminated with an ultraviolet pulsed excimer laser beam at 193 nm. This causes photodissociation of the vinyl cyanide, yielding photoproducts including HCN and HNC.[6] The initially rotationally and translationally hot photoproducts undergo rapid thermalization by frequent collisions with the relatively dense, cold He. The thermalized HCN and HNC are then excited and detected in a time-resolved fashion on the *j*=1-0 transition by a CPFTmmW spectrometer arranged perpendicularly to the flow, yielding the pressure broadening cross-sections as a function of delay time after the excimer laser pulse. At a given time delay after the photolysis laser fires, a short (140—200 ns) pulse of amplified mm-wave radiation is broadcast into the flow from the transmitter, after which the molecular signal (the free induction decay, or FID) is collected and amplified by the receiver and recorded over ~1 μs. After background subtraction these molecular FIDs can be fitted in the time-domain to yield the so-called T_2 relaxation time for each molecule as a function of time delay after its creation by laser photolysis. This delay corresponds to the position in the flow where the molecules were generated, as can be seen in Fig. 1b which shows a typical 2-D density map of the uniform supersonic flow (obtained by impact pressure measurements) above Fig. 1c which displays the measured T_2 relaxation times for HCN and HNC as a function of time after the laser shot. Further details may be found in the Methods section.

Time domain data analysis

The rate of decay of the FID was fitted to obtain the pressure broadening cross sections in these experiments. As described in a recent study,[27] both the time domain and the frequency domain contain the same information, but the effects of interference from hyperfine splitting are more easily accounted for in the time domain. Examples of these fits are shown in Fig. 2 for HCN and HNC. Fig. 2 panels b and d show the FFTs (Fast Fourier Transforms) of both the data and the time domain fit, to show how well the FID decay is captured by the model. A time domain Voigt model was used to fit this data, which also accounts for the hyperfine splitting of HCN that imposes a beat frequency along with the FID. This model is discussed in the Supplementary Material.

The fitted exponential decays are shown in Fig. 2 panel e for HCN and HNC, without any frequency components. It is easily seen that the decay times (T_2) for each of these molecules is different, despite being produced under the same conditions. This is entirely due to the difference in pressure broadening cross section of these two molecules. The T_2 decay times are converted into pressure broadening cross sections $\sigma(T)$ using the precisely known density and temperature of the uniform supersonic flow as described in the Supplementary Materials (Supplementary Eq. 2). Only molecules isolated within the cold uniform flow were included in the pressure broadening data, which could be easily distinguished from molecules produced in the nozzle by time dependent changes of the decay rate at the end of the collected flow data as shown in Fig. 1c.

Theoretical calculations

Several HCN–He and HNC–He potential energy surfaces (PESs) have been published (e.g. Sarrasin et al. 2010 and references therein[15]). However, it is well known that scattering calculations under cold conditions are highly sensitive to the PES accuracy. Hence, using state of the art ab initio methods, we computed highly accurate two-dimensional HCN–He and HNC–He PESs with HCN and HNC intramolecular distances fixed. Theoretical pressure broadening cross sections and rate coefficients for the j = 0 and 1 levels of HCN and HNC were obtained by performing quantum dynamics[28] on these PESs using the MOLSCAT code.[29] Because of the low temperatures considered in this work, a full close-coupling approach was employed to compute the related cross sections.[30] More details on these calculations can be found in the Methods section and in the Supplementary section 'Theoretical calculations'.

The experimentally determined pressure broadening cross sections are compared against those found from scattering calculations from the *ab initio* PESs used for each molecule in Fig. 3. The results are also reported in Supplementary Table 1.

Discussion

The experimental and theoretical pressure broadening cross sections from this work are compared together and against previously available experimental data in Fig. 3. Importantly, these cross sections are presented on an absolute scale, directly calibrating the magnitude of cross sections used in these calculations. The agreement between the experimental data and the scattering calculations from this work over the temperature range 10—70 K is very good. The j=1-0 transition for HCN in He has been experimentally observed on several occasions above 130 K[31] and by Ronningen and de Lucia between 1.3 K and 6.2 K.[32] At higher temperatures, the current calculations agree very well with previous experiments. The highest temperature data from Ronningen and de Lucia are just below the lowest temperature at which the current experiments were performed (10 K). However, it can be seen from Fig. 3 that the calculations predict the cross section to rise as the temperature drops, and that this is confirmed by the current experiments down to 10 K. Other studies have called into question the absolute accuracy of the collisional cooling technique used by Ronningen and de Lucia especially at very low temperatures.[32,33] It should be emphasized, though, that the temperature ranges of the two sets of measurements do not overlap. For the unstable HNC isomer, this is the only pressure broadening study to the authors' knowledge, and so no data were available for comparison. The current experimental cross sections are in very good agreement with the calculated values, with an average RMS deviation of only 18 % and 25 % for the HCN–He and HNC–He cross sections respectively.

The rising trend with decreasing temperature is well reproduced as is the overall magnitude for HNC–He, which is significantly higher than for HCN–He. Pressure broadening cross sections typically do not offer the most sensitive test of PESs and scattering calculations due to the summation of both inelastic and elastic contributions,[34] followed by integration over a thermal distribution of energies to give the temperature-dependent cross sections measured and calculated here. All this averaging normally reduces the sensitivity of these measurements to differences in PESs, though the effect of averaging is diminished at low temperatures. What is so striking about this study is that even after this blurring of the microcanonical processes and the

apparent similarities between HCN and HNC, the *difference* in these systems is still readily apparent from the measurements.

The larger pressure broadening cross sections observed for HNC–He versus HCN–He, especially at very low temperatures, are partly due to the greater well depth for the HNC–He PES versus the HCN–He PES (46.09 versus 30.10 cm^{-1}). Another contributing factor can be understood by examining the state-to-state rate coefficients for inelastic rotational energy transfer out of the j = 0 and 1 levels, which constitute the main contribution to the measured pressure-broadening cross sections. They have been explicitly calculated by Sarrasin et al.,[15] and are displayed for a temperature of 10 K in Supplementary Fig. 2. As noted by Sarrasin et al., the HCN–He system with its less anisotropic potential appears to resemble more closely the case of an "almost homonuclear" diatomic molecule – atom system than does HNC–He, resulting in a propensity for even Δj transitions which is not observed for HNC–He. Such behavior was predicted long ago by McCurdy and Millar[35] in terms of semiclassical theory, as being due to destructive interference in the case of odd Δj transitions. At these low temperatures, the rate coefficients drop strongly with Δj according to the usual exponential gap law, as can be seen for the HNC–He case in Fig. S2, where by far the largest state-to-state rate coefficients are for Δj = +1 and (when possible) Δj = −1. However, in the "almost homonuclear" HCN–He system, the even Δj propensity rule results in a strong suppression of these Δj = ±1 rate coefficients, resulting in a much lower overall pressure broadening cross section. This effect is particularly important at the lowest temperatures where higher positive Δj rate coefficients, corresponding to endoergic processes, are also suppressed. In space, these same processes compete with spontaneous emission from j=1-0, the most commonly monitored transition in astronomical observations of these molecules.[14] The strong difference in inelastic cross sections for j=1-0 between HCN and HNC with He – almost four times – is expected to preferentially pump into the j=1 level for HNC.

The difference between the pressure broadening cross sections for HCN and HNC validates the explanation proposed by Lique and coworkers[14] for the HNC/HCN abundance ratio, at least in the case of one of the main colliders in dark clouds, He atoms. This is further strengthened by the good agreement on an absolute scale between the scattering calculations and experimental measurements. The inelastic rate coefficients calculated previously by Lique and co-workers for these systems[15,17] agree very well with those computed here, differing by less than 5% on the overlapping temperature range. This confirms the validation of these previous results. Both theory and experiment now demonstrate that the assumption of identical RET rate coefficients for the two isomers is incorrect. Similar effects of propensity rules were also predicted for collisions of HCN and HNC with the other main collider, H_2, but only for the *para* (j=0) level.[14] The magnitudes and differences were found to be similar to HCN and HNC with He. Current predictions using these collisional data still find that HNC can be more abundant in some of the coldest regions, hinting at unexplored chemical routes to this overabundance.[36]

Comparison of the isoelectronic systems HCN and N_2H^+ with He have revealed different propensity rules even in such similar cases.[37] Our experiment is the only one to definitively find a difference in an *isomeric* collisional system, but other such examples may be present in the ISM. Several other cyanide/isocyanide species have been explored in theoretical studies.[38–42] Abundance ratios of longer chain cyano/isocyano molecules have been determined in recent observations,[43,44] and these may also be susceptible to different excitation conditions in the same way as for HCN and HNC with He. The pressure broadening of HCN and HNC

at low temperatures may also be of interest for observations of cold planetary atmospheres, such as that of Neptune.[45] The wide variety of HNC/HCN abundance ratios observed in comets (ranging from ~ 0.03 to 0.3) remains puzzling and the formation mechanism of HNC is still unclear.[46,47] Our study demonstrates the importance of specific calculations and measurements of collisional excitation for key astrophysically relevant systems.

The predictions made from high level scattering calculations are often compared against systems that are amenable for experimental measurement, usually employing laser excitation for detection, sometimes combined with velocity map imaging and other sophisticated techniques such as Stark deceleration.[48] While such experiments permit exquisite comparisons between theory and experiment, they are limited to a number of 'model' systems such as NO or OH with established laser detection schemes. The use of a chirped pulse spectrometer allows for a much wider variety of molecules to be probed. The cooling provided by the CRESU technique pushes the available energies into the regime where quantum effects are important, and the fact that the flow density and temperature are precisely known permits absolute measurements, further testing *ab initio* theories.

Conclusions

This study reports the only experiments to date showing that collisional excitation differs between structural isomers at interstellar temperatures. HCN and HNC have been formed together *in situ* in cold He supersonic flows, and a strong difference has been observed in the pressure broadening cross sections for the two isomers, especially at the lowest temperatures. Theoretical calculations of the pressure broadening parameters for HCN and HNC with He have been made to compare against these results, and excellent agreement has been observed on an absolute scale. This confirms previous theoretical arguments of Lique and coworkers regarding the importance of differences in PESs of structural isomers with He, and it is to be expected that other systems should display this too. This is one of the few experiments to specifically address the HCN to HNC abundance in the interstellar medium, with a combination of experimental techniques that allow for both isomers to be probed explicitly.

Acknowledgments

The authors would like to thank Jonathan Courbe, Jonathan Thiévin, Didier Biet, Ewen Gallou, and Alexandre Dapp for technical support, as well as André Canosa for the design of some of the Laval nozzles used in the project. The authors acknowledge funding from the European Union's Horizon 2020 research and innovation programme under the European Research Council (ERC) grant agreement 695724-CRESUCHIRP (I.R.S.) and under the Marie Skłodowska-Curie grant agreement 845165-MIRAGE (I.R.C. and I.R.S.). The authors are also grateful for support from the European Regional Development Fund, the Region of Brittany and Rennes Metropole. This work was supported by the French National Programme "Physique et Chimie du Milieu Interstellaire" (PCMI) of CNRS/INSU with INC/INP co-funded by CEA and CNES.

***Author Contributions Statement*:**

B.M.H. and I.R.S. conceived the project. B.M.H., D.G., T.G., O.A.K. and I.R.C. performed the experiments and analysed the data. F.T. and F.L. performed the theoretical calculations. B.M.H., I.R.S., F.T. and F.L. wrote the paper. All authors contributed to discussions and gave comments on the manuscript.

***Competing Interests Statement*:**

The authors declare no competing interests.

Figure Legends/Captions (for main text figures)

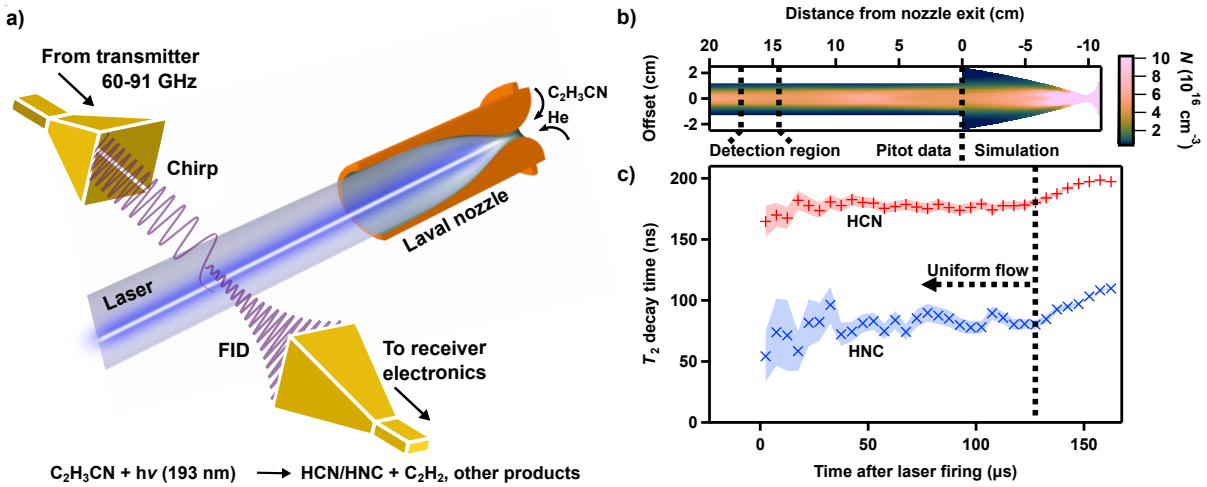

Fig. 1 | Schematic view of the experiment with 2-D density map and T_2 decay times. a, Schematic of the experiment showing a uniform He flow from a Laval nozzle. The cold core of the flow is illuminated by a pulsed 193 nm laser, generating HCN and HNC molecules *in situ* by photolysis of vinyl cyanide, which are then detected downstream from the nozzle exit by the cp-FTmmW spectrometer. **b**, An example 2-D density map taken from Pitot measurements under 16 K conditions in a He flow, showing the higher density isentropic core giving way to the boundary regions, where the density drops rapidly and the temperature increases. Shown are the interpolated data between the original 0.25 × 1 cm point spacing of the experimentally measured grid. The region that the spectrometer probes is indicated. The map is completed by a computational fluid dynamics simulation for the flow within the nozzle using Ansys Fluent, capped at a maximum density of 1×10^{17} cm^{-3} (otherwise the much higher density in the throat of the nozzle would compress the scale of the whole map). **c**, Measurements of the T_2 decay time as a function of time after the laser shot. The time axis is scaled to the distance from the nozzle exit in b, as under uniform conditions the molecules moving through the detection zone will be formed at a given position that can be correlated to time. The shaded areas around the T_2 decay times represent the 95% confidence intervals for fitting the Voigt profile at each point along the uniform flow. Each T_2 decay time results from fitting of an FID which is an average of 10^5 laser shots. The difference in T_2 decay times for the two isomers can be clearly seen.

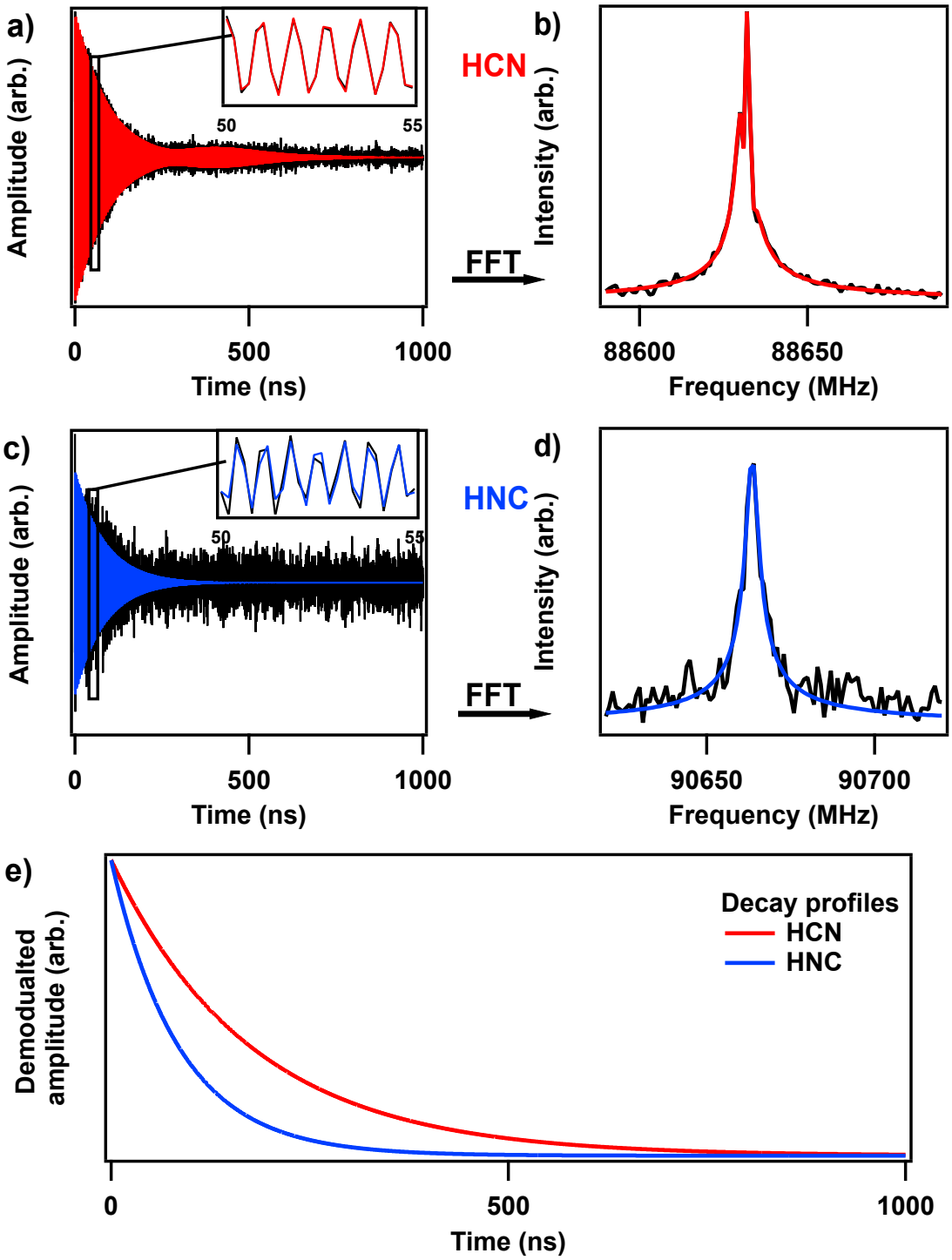

Fig. 2 | Examples of fits to FIDs for HCN and HNC in He at 16 K. a, Time domain experimental data (black) and the fit (red) obtained using Supplementary Eq. 1 for HCN. The inset shows a zoomed version for 5 ns. **b,** FFTs of the data and the fit for HCN shown in panel a. **c**, Time domain experimental data (black) and the fit (blue) obtained for HNC using a time domain Voigt single frequency function as in Hays et al.[27] **d**, FFTs of the data and the fit for HNC shown in panel c. **e**, demodulated decay profiles of fitted data for HCN (red) and HNC (blue). Panels b and d show the FFT of the time domain fits which represent the FFTs of the original data well, highlighting the robustness of fitting the time-domain data. The demodulated decay profiles for each molecule shows the fitted exponential decays of the frequency components for the molecules. The decay times (T_2), recorded under similar conditions, are clearly different, with the decay being faster for HNC than for HCN, reflecting the different He pressure broadening cross-sections. All data displayed result from the averaging of FIDs recorded from 10^5 laser shots.

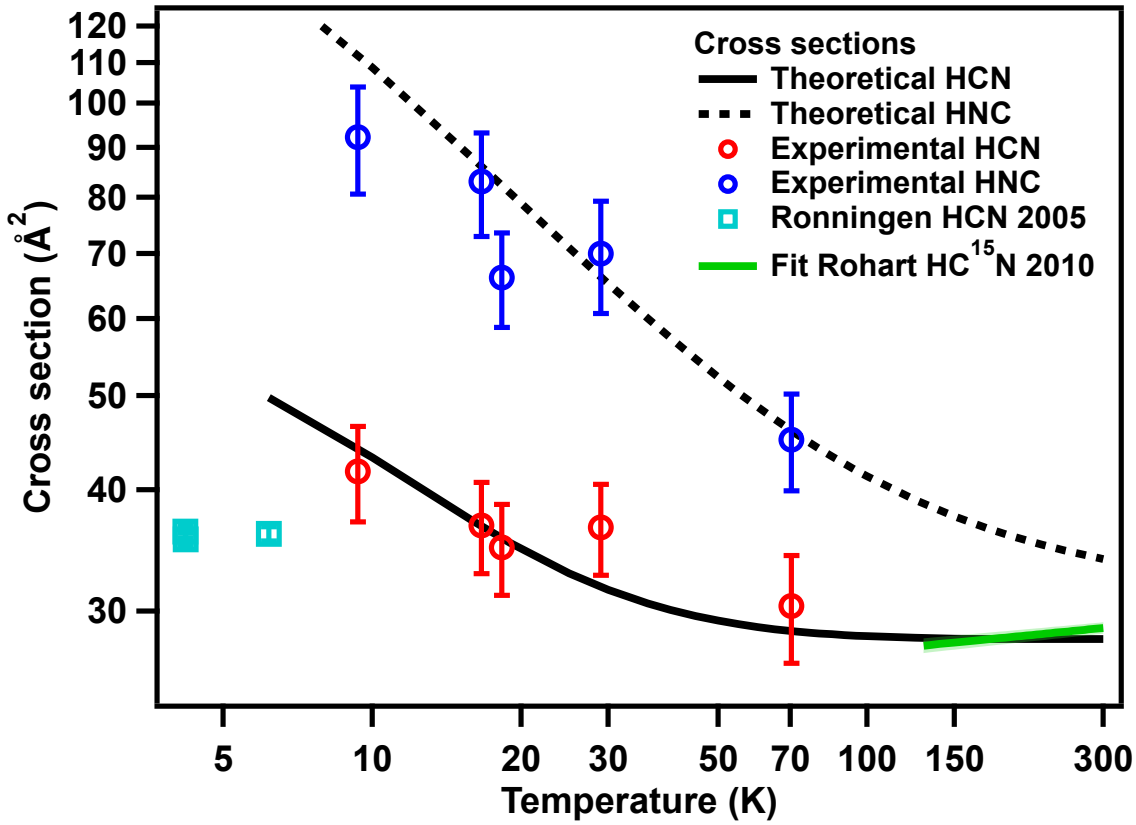

Fig. 3 | Theoretical and experimental pressure broadening cross sections for HCN and HNC with He. Results from this study are compared to those from other experiments, including empirical fits to $HC^{15}N$ data. Error bars for the current experiments correspond to 95% confidence intervals from the averaging of the measured T_2 decay times combined with contributions from estimated possible systematic errors in the flow density and temperature of 10% (see Supplementary Section 1A for further details). Error bars from other work correspond to 2σ when available. Previous data for HCN are from Ronningen and de Lucia 2005[32] and Rohart and Kaghat 2010.[31] The new experimental data and scattering calculations display very good agreement over the temperature range 10—70 K. Both the species show a rising trend in pressure broadening cross sections with decreasing temperature, with the cross sections for HNC being higher than for HCN over this temperature range. This reflects a stronger collisional excitation of HNC than HCN by He (and by implication H_2), especially at the low temperatures found in dense interstellar clouds. This strongly affects the observed HNC/HCN abundance ratio and helps explain anomalously high values that have previously been reported.

References

1. Nguyen, T. L., Baraban, J. H., Ruscic, B. & Stanton, J. F. On the HCN – HNC Energy Difference. *J. Phys. Chem. A* **119**, 10929–10934 (2015).
2. Baraban, J. H. *et al.* Spectroscopic characterization of isomerization transition states. *Science* **350**, 1338–1342 (2015).
3. Makhnev, V. Yu. *et al.* High Accuracy ab Initio Calculations of Rotational–Vibrational Levels of the HCN/HNC System. *J. Phys. Chem. A* **122**, 1326–1343 (2018).
4. Maki, A. G. & Sams, R. L. High temperature, high resolution infrared spectral measurements on the HNC–HCN equilibrium system. *J. Chem. Phys.* **75**, 4178–4182 (1981).
5. Mendes, M. B. *et al.* Cold electron reactions producing the energetic isomer of hydrogen cyanide in interstellar clouds. *Astrophys. J.* **746**, L8 (2012).
6. Prozument, K. *et al.* Photodissociation transition states characterized by chirped pulse millimeter wave spectroscopy. *Proc. Natl. Acad. Sci.* **117**, 146–151 (2020).
7. Loison, J.-C., Wakelam, V. & Hickson, K. M. The interstellar gas-phase chemistry of HCN and HNC. *Mon. Not. R. Astron. Soc.* **443**, 398–410 (2014).

8. Hacar, A., Bosman, A. D. & van Dishoeck, E. F. HCN-to-HNC intensity ratio: a new chemical thermometer for the molecular ISM. *Astron. Astrophys.* **635**, A4 (2020).
9. Long, F. *et al.* Exploring HNC and HCN line emission as probes of the protoplanetary disk temperature. *Astron. Astrophys.* **647**, A118 (2021).
10. Hirota, T., Yamamoto, S., Mikami, H. & Ohishi, M. Abundances of HCN and HNC in Dark Cloud Cores. *Astrophys. J.* **503**, 717–728 (1998).
11. Barger, T., Wodtke, A. M. & Bowman, J. M. Radiative Relaxation and Isomeric Branching of Highly Excited H/C/N: The Importance of Delocalized Vibrational States. *Astrophys. J.* **587**, 841 (2003).
12. Herbst, E., Terzieva, R. & Talbi, D. Calculations on the rates, mechanisms, and interstellar importance of the reactions between C and NH_2 and between N and CH_2. *Mon. Not. R. Astron. Soc.* **311**, 869–876 (2000).
13. Graninger, D. M., Herbst, E., Öberg, K. I. & Vasyunin, A. I. The HNC/HCN ratio in star-forming regions. *Astrophys. J.* **787**, 74 (2014).
14. Hernández Vera, M., Lique, F., Dumouchel, F., Hily-Blant, P. & Faure, A. The rotational excitation of the HCN and HNC molecules by H_2 revisited. *Mon. Not. R. Astron. Soc.* **468**, 1084–1091 (2017).
15. Sarrasin, E. *et al.* The rotational excitation of HCN and HNC by He: new insights on the HCN/HNC abundance ratio in molecular clouds. *Mon. Not. R. Astron. Soc.* **404**, 518–526 (2010).
16. Denis-Alpizar, O., Kalugina, Y., Stoecklin, T., Vera, M. H. & Lique, F. A new ab initio potential energy surface for the collisional excitation of HCN by para- and ortho-H_2. *J. Chem. Phys.* **139**, 224301 (2013).
17. Dumouchel, F., Faure, A. & Lique, F. The rotational excitation of HCN and HNC by He: temperature dependence of the collisional rate coefficients. *Mon. Not. R. Astron. Soc.* **406**, 2488–2492 (2010).
18. Dumouchel, F., Kłos, J. & Lique, F. The rotational excitation of the interstellar HNC by para- and ortho-H_2. *Phys. Chem. Chem. Phys.* **13**, 8204–8212 (2011).
19. Wilhelm, M. J. *et al.* Is Photolytic Production a Viable Source of HCN and HNC in Astrophysical Environments? A Laboratory-based Feasibility Study of Methyl Cyanoformate. *Astrophys. J.* **849**, 15 (2017).
20. Wilhelm, M. J. & Dai, H.-L. Collisional Energy Transfer from Vibrationally Excited Hydrogen Isocyanide. *J. Phys. Chem. A* **123**, 6927–6936 (2019).
21. Prozument, K. *et al.* A new approach toward transition state spectroscopy. *Faraday Discuss.* **163**, 33–57 (2013).
22. Brown, G. G. *et al.* A broadband Fourier transform microwave spectrometer based on chirped pulse excitation. *Rev. Sci. Instrum.* **79**, 053103 (2008).
23. Park, G. B., Steeves, A. H., Kuyanov-Prozument, K., Neill, J. L. & Field, R. W. Design and evaluation of a pulsed-jet chirped-pulse millimeter-wave spectrometer for the 70–102 GHz region. *J. Chem. Phys.* **135**, 024202 (2011).
24. Abeysekera, C. *et al.* A chirped-pulse Fourier-transform microwave/pulsed uniform flow spectrometer. II. Performance and applications for reaction dynamics. *J. Chem. Phys.* **141**, 214203 (2014).
25. Rowe, B. R., Dupeyrat, G., Marquette, J. B. & Gaucherel, P. Study of the reactions $N_2^+ + 2N_2 \rightarrow N_4^+ + N_2$ and $O_2^+ + 2O_2 \rightarrow O_4^+ + O_2$ from 20 to 160 K by the CRESU technique. *J. Chem. Phys.* **80**, 4915–4921 (1984).
26. Sims, I. R. *et al.* Rate constants for the reactions of CN with hydrocarbons at low and ultra-low temperatures. *Chem. Phys. Lett.* **211**, 461–468 (1993).
27. Hays, B. M. *et al.* Design and performance of an E-band chirped pulse spectrometer for kinetics applications: OCS – He pressure broadening. *J. Quant. Spectrosc. Radiat. Transf.* **250**, 107001 (2020).
28. Arthurs, A. M. & Dalgarno, A. The theory of scattering by a rigid rotator. *Proc. R. Soc. Lond. Ser. Math. Phys. Sci.* **256**, 540–551 (1960).

29. Hutson, J. & Green, S. MOLSCAT computer code, version 14, distributed by Collaborative Computational Project No. 6 of the Engineering and Physical Sciences Research Council. *Swindon UK* (1994).
30. Shafer, R. & Gordon, R. G. Quantum scattering theory of rotational relaxation and spectral line shapes in H_2–He gas mixtures. *J. Chem. Phys.* **58**, 5422–5443 (1973).
31. Rohart, F. & Kaghat, F. HCN absorption line shapes studied by millimeter wave coherent transients: speed dependent effects and collision interaction potential. *AIP Conf. Proc.* **1290**, 209–213 (2010).
32. Ronningen, T. J. & De Lucia, F. C. Helium induced pressure broadening and shifting of HCN hyperfine transitions between 1.3 and 20 K. *J. Chem. Phys.* **122**, 184319 (2005).
33. Thachuk, M., Chuaqui, C. E. & Le Roy, R. J. Linewidths and shifts of very low temperature CO in He: A challenge for theory or experiment? *J. Chem. Phys.* **105**, 4005–4014 (1996).
34. Ben-Reuven, A. Impact Broadening of Microwave Spectra. *Phys. Rev.* **145**, 7–22 (1966).
35. McCurdy, C. W. & Miller, W. H. Interference effects in rotational state distributions: Propensity and inverse propensity. *J. Chem. Phys.* **67**, 463–468 (1977).
36. Riaz, B., Thi, W.-F. & Caselli, P. Chemical tracers in proto-brown dwarfs: CN, HCN, and HNC observations. *Mon. Not. R. Astron. Soc.* **481**, 4662–4679 (2018).
37. Pursell, C. J., Weliky, D. P. & Oka, T. Collision-induced double resonance studies of HN^+_2 and HCN. *J. Chem. Phys.* **93**, 7041–7048 (1990).
38. Hernández Vera, M. *et al.* Cyanide/isocyanide abundances in the interstellar medium – II. Inelastic rate coefficients of Al and Mg compounds. *Mon. Not. R. Astron. Soc.* **432**, 468–477 (2013).
39. Hernández Vera, M. & Lique, F. Cyanide/isocyanide abundances in the interstellar medium – III. The excitation of Al and Mg compounds. *Mon. Not. R. Astron. Soc.* **448**, 2438–2447 (2015).
40. Hernández Vera, M., Lique, F., Kłos, J., Dumouchel, F. & Rubayo Soneira, J. Cyanides/isocyanides abundances in the interstellar medium – IV. Temperature dependence of SiCN/SiNC rate coefficients and astrophysical applications. *Mon. Not. R. Astron. Soc.* **451**, 1199–1211 (2015).
41. Senent, M. L., Dumouchel, F. & Lique, F. Cyanide/isocyanide abundances in the interstellar medium – I. Theoretical spectroscopic characterization. *Mon. Not. R. Astron. Soc.* **420**, 1188–1194 (2012).
42. Bop, C. T. *et al.* Isomerism Effects in the Collisional Excitation of Cyanoacetylene by Molecular Hydrogen. *ACS Earth Space Chem.* **3**, 1151–1157 (2019).
43. Cernicharo, J. *et al.* Discovery of HC_4NC in TMC-1: A study of the isomers of HC_3N, HC_5N, and HC_7N. *Astron. Astrophys.* **642**, L8 (2020).
44. Xue, C. *et al.* Detection of Interstellar HC_4NC and an Investigation of Isocyanopolyyne Chemistry under TMC-1 Conditions. *Astrophys. J.* **900**, L9 (2020).
45. Rezac, L. *et al.* New determination of the HCN profile in the stratosphere of Neptune from millimeter-wave spectroscopy. *Astron. Astrophys.* **563**, A4 (2014).
46. Mumma, M. J. & Charnley, S. B. The Chemical Composition of Comets—Emerging Taxonomies and Natal Heritage. *Annu. Rev. Astron. Astrophys.* **49**, 471–524 (2011).
47. Lis, D. C. *et al.* Hydrogen Isocyanide in Comet 73P/Schwassmann-Wachmann (Fragment B). *Astrophys. J.* **675**, 931–936 (2008).

Methods

Experimental

He buffer gas (Air Liquide 99.995%) is flowed through convergent-divergent de Laval nozzles, which were aerodynamically shaped to form cold supersonic uniform flows. Four de Laval nozzles were used to produce five temperatures around 10, 16, 19, 30, and 70 K in uniform flows with densities varying between 0.2—1 ×

10^{17} cm^{-3}, each temperature condition having a specific density that varies by less than 10% over the probing region. Measured temperatures and densities are given in Supplementary Table 1. Conditions within the flows were precisely controlled using mass flow controllers (Brooks SLA5851S) and through pressure measurements using capacitance manometers (Brooks XacTorr CMX0). The temperature and density of the uniform flow from each de Laval nozzle were characterized by impact pressure measurements through the Rayleigh relations in isentropic flow.[49]

HCN and HNC were prepared by pulsed excimer laser photolysis of vinyl cyanide (acrylonitrile, Sigma Aldrich >99% purity) at 193 nm (Coherent LPX Pro 210 F) at a 100 Hz repetition rate with a laser fluence in the observation region of typically 30 mJ cm^{-2}. This produces both molecules at relatively high abundance.[6] Vinyl cyanide was entrained in the flow at low densities (~0.1% of the total), via a Coriolis liquid flow controller (Bronkhorst mini CORI-FLOW ML120V00) and a Controlled Evaporative Mixer (CEM, Bronkhorst W-202A-222-K) as described previously.[50] The laser photolysis products are rotationally cooled by collisions to low temperatures under the CRESU conditions, providing a cold sample to probe spectroscopically. The laser was aligned along the center of the flow and constrained in size to specifically interact with molecules only in the isentropic core and not the surrounding warmer boundary layers.[51]

The ground vibrational state *j*=1-0 transitions of HCN and HNC were probed in the CRESU flows using an E-band CP-FTmmW spectrometer which has been recently described in detail.[27] Here, it was adapted for spectroscopy under CRESU conditions in a specially constructed vacuum chamber. The spectrometer operates between 60-90 GHz but was able to extend the range to observe HNC. The rectangular feedhorns were mounted inside the vacuum chamber perpendicularly to the uniform flow, and situated 10 or 16 cm downstream from the exit of the de Laval nozzles to probe the uniform portion of the cold flow.

The arbitrary waveform generator (Keysight M8195A) and digitizer (Teledyne SP Devices ADQ7DC-PCIE) used in these experiments were the same as in previous works[27,51] but were reconfigured for time resolved acquisition following pulsed laser photolysis in the uniform flow. 400 μs pulse train sequences were used with 2.5 μs long pulse/collection cycles, resulting in 160 individual pulse – FID (Free Induction Decay) cycles per train, with the laser firing after the first half of each sequence. The first 80 cycles of each sequence were averaged together to produce an averaged background without any molecular signals. This background was subtracted from each cycle after the laser fired, allowing for the molecular FID to be differentiated from the reflections inherent in the system. When performing background subtractions, a slight phase shift[23] of each cycle was performed to increase rejection of reflections. When the SNR on a single FID was too low for fitting in the time domain, 2—4 sequential cycles were horizontally averaged before fitting, increasing the SNR of a scan but blurring the time resolution within the pulse sequence after the laser fired. This combines aspects of both segmented averaging[52] and FastFrame® [24] in a custom acquisition scheme. A total of 10^5 laser shot – pulse train sequences were averaged together at 100 Hz, taking about 15 minutes per experiment. At 70 K four of these experiments were averaged together due to lower population in the probed levels.

Theoretical

The PESs were calculated in the supermolecular approach by means of the explicit correlated coupled cluster method including single, double, and perturbative triple excitations [CCSD(T)-F12a][53] with an augmented correlation-consistent polarized valence triple-ζ [aug-cc-pVTZ] basis set[54] (hereafter CCSD(T)-F12/aug-cc-pVTZ). After fitting of the interaction energy, close coupling scattering calculations were performed on these PESs to find the pressure broadening cross sections. More details on these calculations can be found in Supplementary section 2 'Theoretical calculations'.

Data availability

The source data for all the Figures in the main article and in the Supplementary Information, as well as the source data for the experimental and theoretical cross sections are publicly available in the Zenodo data repository[55] at https://doi.org/10.5281/zenodo.6256226

Code availability

The codes used to analyse the experimental data and generate the theoretical data presented in this study are publicly available in the the Zenodo data repository[55] at https://doi.org/10.5281/zenodo.6256226, or via the cited references.

References (for Methods section only)

48. de Jongh, T. *et al.* Imaging the onset of the resonance regime in low-energy NO-He collisions. *Science* **368**, 626–630 (2020).
49. Dupeyrat, G., Marquette, J. B. & Rowe, B. R. Design and testing of axisymmetric nozzles for ion-molecule reaction studies between 20 °K and 160 °K. *Phys. Fluids* **28**, 1273–1279 (1985).
50. Gupta, D. *et al.* Low Temperature Kinetics of the Reaction Between Methanol and the CN Radical. *J. Phys. Chem. A* **123**, 9995–10003 (2019).
51. Hearne, T. S., Abdelkader Khedaoui, O., Hays, B. M., Guillaume, T. & Sims, I. R. A novel Ka-band chirped-pulse spectrometer used in the determination of pressure broadening coefficients of astrochemical molecules. *J. Chem. Phys.* **153**, 084201 (2020).
52. Neill, J. L. *et al.* Segmented chirped-pulse Fourier transform submillimeter spectroscopy for broadband gas analysis. *Opt. Express* **21**, 19743–19749 (2013).
53. Knizia, G., Adler, T. B. & Werner, H.-J. Simplified CCSD(T)-F12 methods: Theory and benchmarks. *J. Chem. Phys.* **130**, 054104 (2009).
54. Kendall, R., Dunning, T. & Harrison, R. Electron-Affinities of the 1st-Row Atoms Revisited - Systematic Basis-Sets and Wave-Functions. *J. Chem. Phys.* **96**, 6796–6806 (1992).
55. Hays, B. M. *et al.* Data for Hays et al. Nature Chemistry 2022, NCHEM- 21050864A. (2022) doi:10.5281/zenodo.6256226.